Malaysian Journal of Pharmaceutical Sciences
Vol. 21, No. 1, 63–89 (2023)

IN SILICO EVALUATION OF AROMATASE INHIBITORY ANTI-BENIGN PROSTATIC HYPERPLASIA POTENTIALS OF SPIROSTAN SAPOGENINS

OLUSEGUN SAMSON AJALA*, MOSHOOD OLUSOLA AKINLEYE, MBANG OWOLABI AND GRACE UKPO
Department of Pharmaceutical Chemistry, Faculty of Pharmacy,
University of Lagos, Nigeria

Published online: 25 May 2023
To cite this article: AJALA, O. S., AKINLEYE, M. O., OWOLABI, M. & UKPO, G. (2023) *In silico* evaluation of aromatase inhibitory anti-benign prostatic hyperplasia potentials of spirostan sapogenins, *Malaysian Journal of Pharmaceutical Sciences*, 21(1): 63–89, https://doi.org/10.21315/mjps2023.21.1.5
To link to this article: https://doi.org/10.21315/ mjps2023.21.1.5

ABSTRACT

Inherent oestrogen receptor alpha (ERα) and other nuclear receptor signaling activities of typical aromatase inhibitors (AIs) preclude their clinical use as anti-oestrogenic anti-benign prostatic hyperplasia (anti-BPH) agents. Spirostan sapogenins (SS) constitute a chemical space from which AIs without such deterrents could be sought. This work was aimed at in silico discovery of clinical aromatase inhibitory anti-oestrogenic anti-BPH drug leads. Forty-six SS were docked against an inhibitor conformation of the human placenta aromatase. Nuclear receptor signaling activation tendencies of seven of them showing high docking scores comparable to that of the co-crystalised ligand, exemestane, were determined in a ligand-based webserver screening (Protox-II) and docking against an agonist conformation of the ERα ligand binding domain (ERαLBD). Other toxicity and pharmacokinetic/drug-likeness evaluations were caried out using Protox-II and SwissADME webservers. Stability of aromatase complex with the highest-docking-score SS was explored in a molecular dynamics simulation using Webgro molecular dynamics webserver at a 20 ns simulation time. None of the seven SS activated the nuclear receptor signaling pathways; pharmacokinetic/drug-likeness predictors showed that they would be orally bioavailable; they were not susceptible to drug metabolising cytochrome P450 (CYP) isozymes and two of them demonstrated non-susceptibility to the efflux transport activity of P-glycoprotein (Pgp). Molecular dynamics data analysis revealed the root mean square deviation (RMSD) of 2 Å–3 Å and a radius of gyration of and 22 Å over the 20 ns simulation time. This investigation provides a molecular framework for anti-oestrogenic anti-BPH therapeutic strategy via aromatase inhibition (AI) and unmasks seven SS as potential anti-BPH AIs.

***Keywords*:** Spirostan sapogenins, *In silico* ADMET studies, Benign prostatic hyperplasia, Aromatase inhibitos, *In silico* drug discovery

*Corresponding author: olajala@unilag.edu.ng

INTRODUCTION

Benign prostatic hyperplasia (BPH) is the non-neoplastic of the two proliferative diseases of the prostate gland, the second being prostate cancer (Sciarra et al. 2008; Elkahwaji 2013). Though its molecular etiology is not yet clearly understood, its endocrine undertone is unequivocal (La Vignera 2016). It was initially exclusively associated with the male sex hormones responsible for the development of secondary male characteristics—the androgens. This androgen theory especially implicates dihydrotestosterone, the major metabolite of testosterone often found accumulated in the prostate and which also formed the basis for the anti-androgenic 5α-reductase inhibition strategy of BPH management (Andriole 2004). The androgen theory and its ensuing 5α-reductase inhibition therapeutic strategy, however, have a number of issues. Asides the major unbearable side effects of 5α-reductase inhibition, it does not work in all cases of BPH (Montironi, Valli and Fabris 1996; Trost, Saitz and Hellstrom 2013; Hirshburg et al. 2016, Saengmearnuparp et al. 2021). In addition, the marked decrease in concentration of testosterone and other androgens with aging in men does not add up at all to the increase in BPH incidence with aging (Kaplan et al. 2013; Rastrelli et al. 2019). Moreover, though androgens have been experimentally linked with the prostate development, their link to either induction or progression of BPH is still a matter of controversy. At best, the androgen theory in BPH establishment and progression is, today, largely rationalised as merely permissive, giving credence and prominence to the hitherto less considered alternative—the oestrogen theory (Ho and Habib 2011).

Oestrogens are formed in virtually all tissues of the body as metabolites of androgens in an aromatisation bioconversion process catalysed by the enzyme aromatase (Barakat et al. 2016). This portends extra-gonadal oestrogen functions, showing that oestrogens are in no way female-specific and that androgens may after all be merely serving as oestrogen precursors in many of androgen-ascribed male-specific phenomena like BPH. Moreover, oestrogen concentration and BPH incidence have both been reported to increase significantly with aging (Ho and Habib 2011), more or less implicating oestrogens in both health and disease of the prostate. Anti-oestrogen or oestrogen deprivation medical treatment of BPH is therefore, for many reasons, desirable and eagerly anticipated in clinical medicine to revolutionise BPH management.

Aromatase inhibition (AI) is the most specific medical oestrogen ablation/deprivation therapeutic strategy that has been successfully deployed in the management of a number of oestrogen-dependent diseases, including post-menopausal breast cancer, anovulatory infertility and endometriosis (Mitwally and Casper 2006; Pavone and Bulun 2012; Sabale, Sabale and Potey 2018). However, despite several hypotheses and experimental investigations supporting possible clinical management of BPH via aromatase inhibition (Henderson 1987; Henderson et al. 1987; Etreby et al. 1991), no AI has yet been used in the medical treatment of BPH, which indeed has no anti-oestrogenic agent but instead consists mainly of the rather anti-androgenic 5α reductase inhibitors and α1-adrenoceptor blockers (Bechis et al. 2014; Lokeshwar et al. 2019). And although, many are the shortcomings of typical AIs limiting their use in clinical medicine (Howell and Cuzick 2005; Gaillard and Stearns 2011), perhaps the only one deterring their clinical application in BPH management is their nuclear receptor protein superfamily signaling pathways activation/induction. The negative effect of this activation hardly exceeds being merely a resistance problem in most of the clinical applications of AIs (Flågeng et al. 2009; Fujii et al. 2014; Lui et al. 2016; Hanamura and Hayashi 2018). However it could be consequentially grave in prostate affairs, given the oestrogenic homeostatic control of prostatic mitosis via two rather opposing but unevenly distributed

oestrogen receptor isoforms, oestrogen receptor alpha (Erα) and oestrogen receptor beta (Erβ). While ERα effects in the prostate are majorly those of inflammation and cellular proliferation, prostatic ERβ effects are basically pro-apoptotic (Ellem and Risbridger 2009). Skewing this balance by AIs' ERα signaling would, therefore, worsen the progression of an already established BPH, their primary oestrogen ablation properties notwithstanding. Thus, AI without the attendant activation of ERα and other nuclear receptor signaling pathways would renew the hope of medical oestrogen ablation in the clinical management of BPH. To this end, we conjectured that spirostan sapogenins (SS), also simply referred to as spirostans, are a group of natural compounds in which structural novelties required for such intricate biological activities could be repository.

Table 1: QSAR predictions of anti-proliferative, specific anti-BPH and aromatase inhibitory anti-BPH mechanistic tendencies of 15 representative spirostans. Activity potentials are expressed to the nearest 100th of probabilities.

S/N	Compound	Probability of potential activity (to the nearest 100th)							
		ABPH*	APDA*	APRD*	APAA*	AINA*	ANPA*	APCA*	ARIA*
1	Solancarpidine	0.39	0.57	0.52	0.46	0.92	0.91	0.20	0.07
2	Tomatidine	0.31	0.45	0.34	0.42	0.89	0.86	–	–
3	Ketotigogenin	0.40	0.57	0.82	0.90	0.86	0.85	0.45	0.20
4	Smilagenin	0.34	0.51	0.83	0.90	0.71	0.87	0.45	0.08
5	Hecogenin	0.34	0.52	0.90	0.90	0.71	0.90	0.45	0.13
6	Sarsasapogenin	0.34	0.51	0.83	0.90	0.71	0.87	0.45	0.08
7	Solasodine diacetate	0.41	0.56	0.59	0.49	0.82	0.81	0.31	0.12
8	Brisbagenin	0.31	0.48	0.83	0.90	0.69	0.90	0.44	0.04
9	Cannigenin	0.31	0.48	0.83	0.90	0.69	0.90	0.44	0.04
10	Mexogenin	0.34	0.49	0.88	0.60	0.78	0.90	0.46	0.05
11	Convallagenin	0.24	0.45	0.90	0.90	0.57	0.89	0.47	–
12	Convallamarogenin	0.31	0.51	0.82	0.88	0.68	0.92	0.38	0.07
13	Yamogenin	0.41	0.60	0.93	0.85	0.77	0.85	0.49	0.18
14	Anzurogenin A	0.26	0.42	0.88	0.87	0.71	0.89	0.45	–
15	Ruizgenin	0.31	0.48	0.82	0.89	0.73	0.89	0.49	0.05

Notes: *ABPH = anti-benign prostatic hyperplasia activity; *APDA = anti-prostate disorder activity; *APRD = anti-proliferative disease activity; *APAA = apoptosis agonist activity; *AINA = anti-inflammatory activity; *ANPA = antineoplastic activity; *APCA = anti-prostate cancer activity; *ARIA = aromatase inhibitory activity.

SS (or spirostans) are steroid aglycones of saponins consisting essentially of the basic steroidal cyclopentanoperhydrophenanthrene nucleus and a side chain made up of two heterocycles—tetrahydrofuran and tetrahyropyran—connected in a spiroketal fashion at the C-22 position (Figure 2) (Bhat, Nagasampagi and Sivakumar 2005). Though there is but limited structural variations amidst the spirostans, their spiroketal moiety is enough structural novelty that could confer on them intricate biological activities not seen in other steroidal compounds. In the current research, we conjectured, on account of steroidal nature, that SS could inhibit the aromatase, whose natural substrates—testosterone and androstenedione—are also essentially steroidal (Séralini and Moslemi 2001). Moreover, we further conjectured that, on account of the unique spirostan steroidal side chain, macromolecular interaction with the SS would significantly differ from those of other steroids and would most likely not excite ERα as reported for typical AIs.

These conjectures were evaluated in silico by docking 46 SS randomly retrieved from the Pubchem chemical database (Table 1) against an inhibitor conformation model of the human aromatase retrieved from the RCSB Protein databank (Figure 1). Using ligand-based toxicity predictors of a suitable webserver (Protox II), ERα and nuclear receptors signaling activation were predicted for seven spirostans (digitogenin, mannogenin, ketotigogenin, brisbagenin, hecogenin, spirost-1-en-3-one and yuccogenone) demonstrating high aromatase-binding affinities (Figure 2). Their ERα-sparing potential in particular was structurally corroborated by docking them against the human oestrogen receptor alpha ligand binding domain (ERαLBD) model downloaded from the PDB (Figure 3). Pharmacokinetics and drug-likeness of these ligands were predicted using absorption, distribution, metabolism and excretion (ADME) predictor models of the SwissADME webserver. The stability of the aromatase-SS complex with the highest docking score was also explored by molecular dynamics simulations.

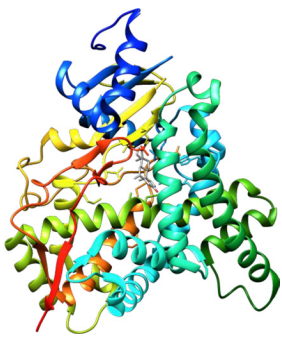

Figure 1: X-ray crystal structure of the human placental aromatase in complex with an inhibitor, exemestane.

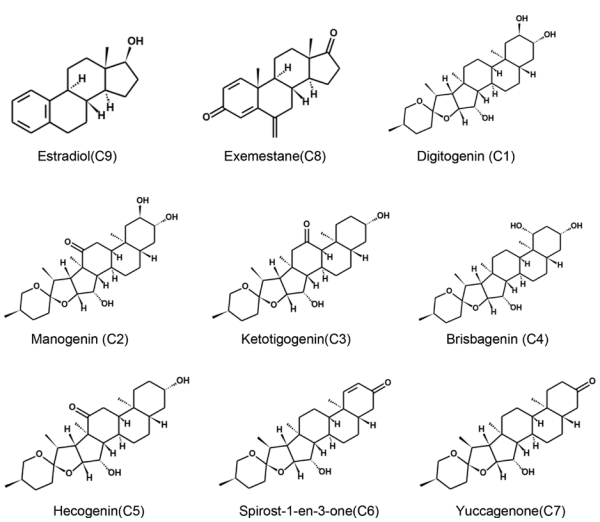

Figure 2: 2D structures of estradiol, exemestane and seven spirostans with aromatase-binding energies comparable to exemestane's.

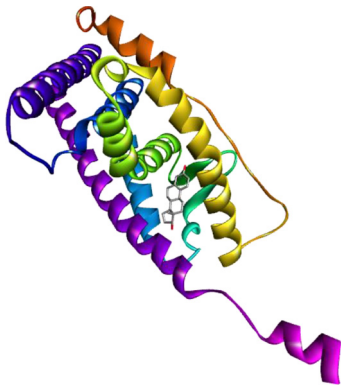

Figure 3: X-ray crystal structure of the human ERαLBD in complex with a natural agonist, estradiol. (Downloaded from RCSB Protein Databank, PDB) (PDBID1A52; 2.80 Å resolution).

METHODS

Hardware, Softwares and Webservers

An HP Probook equipped with intel Core i5, 500 GB hard disk, 8 GB RAM and WiFi was the main hardware used for this work. UCSF Chimera 1.14 (https://www.cgl.ucsf.edu/chimera/) was used for protein preparations; macromolecule-ligand complex simulations and visualisations were done with the aid of BIOVIA Discovery Studio Visualizer 2021 (https://discover.3ds.com/discovery-studio-visualizer-download) and UCSF Chimera 1.14; multiple ligand dockings were carried out using the PyRx molecular docking software with Autodock vina and Open Babel plugins (https://pyrx.sourceforge.io/); Bioinformatics webservers visited for information, downloads and a number of online data processing include RCSB Protein Databank (https://www.rcsb.org/), Pubchem (https://pubchem.ncbi.nlm.nih.gov), SwissADME (http://www.swissadme.ch), Protox II (https://tox-new.charite.de/), CASTp (http://sts.bioe.uic.edu/), UniprotKB (https://www.uniprot.org/help/uniprotkb), Passonline (http://way2drug.com/passonline/) and Webgro molecular dynamics webserver (https://simlab.uams.edu/).

Quantitative Structure Activity Relationship (QSAR)

Using the Passonline webserver, the SS anti-BPH and its aromatase inhibitory action mechanism propositions were consolidated by QSAR predictions for 15 SS, covering general antiproliferative, specific anti-BPH and aromatase-inhibiting tendencies. Specifically, the canonical SMILES (David *et al.* 2020) of each of the 15 SS was fed into the search algorithm of the webserver in succession, monitoring output as probabilities (to the nearest 100th) of each compound's anti-BPH, related cellular proliferation-deterring activities such as anti-prostate disorder, anti-proliferative disease, apoptosis-inducing, antineoplastic, anti-prostate cancer and the action mechanism anti-BPH aromatase inhibitory activities, amongst a host of therapeutic activities listed in the software.

Ligands and Proteins Preparations

Three dimensional (3D) structure data files (sdf) of 46 SS, exemestane and estradiol retrieved from the Pubchem chemical database (Table 2) were uploaded in succession to the PyRx ligand preparation workspace. Energy minimisation and subsequent conversion to autodock-compliant (pdbqt) ligands were performed using the Open Babel plugin in the PyRx software. As at the time of our search, the highest resolution inhibitor conformation aromatase model of human origin in the Protein Databank (PDB) was the human placental aromatase in complex with exemestane (PDB ID 3s7s, Resolution 3.21 Å) (Figure. 1). It was uploaded to the UCSF Chimera 1.14 workspace by direct fetch from the PDB. All non-standard residues, including water, were removed. Hydrogen atoms, which ordinarily do not come with X-ray Crystal models were added as amber charges. Energy minimisation algorithms were run at 200 and 10 steepest descent and conjugate gradient steps, respectively. The prepared protein was saved as a PDB file for subsequent uses. The above protein preparation procedure was followed to prepare a monomer of the human ERαLBD homodimer co-crystalised with the natural activator, estradiol (PDB ID 1A52) (Figure 3).

Docking Validations

Docking to aromatase was validated by re-docking its co-complex inhibitor, exemestane, comparing the binding energy of the ensuing complex with those formed by the spirostans. In the same vein, ERαLBD docking protocol was validated by re-docking its co-crystalised activator, estradiol.

Multiple Ligands Docking to Aromatase and ERαLBD

Forty-six spirostans were docked to aromatase using the PyRx autodock vina plugin algorithm. Seven of the spirostans with high binding affinities comparable to exemestane's were subsequently docked to the agonist conformation of the ERαLBD carrying along exemestane for comparison purposes. Docking sites were identified using active site amino acid residues information garnered from Computed Atlas of Surface Topology of proteins (CASTp), UniprotKB databases and two dimensional (2D) protein-ligand complex visualisations using Discovery Studio. Gridbox coordinates were set for each protein using the autodock vina plugin in PyRx. Aromatase gridbox coordinates were: centre *x* = 87.7887310683; centre *y* = 54.4601539462; centre *z* = 47.1181861287; size *x* = 32.3557572313; size *y* = 23.8423355237 and size *z* = 20.7004087755, while those of the ERα were set as: centre_*x* = 106.597285143; centre_*y* = 16.4207441595; centre_*z* = 97.0734758047; size_*x* = 21.2511938773; size_*y* = 25.9917510005; size_*z* = 24.7189189486. Proteins were set in the two cases as rigid structures while leaving the ligands flexible. Protein-ligand complex stabilities were assessed based on their binding free energies (ΔG).

In silico Toxicity and Pharmacokinetics/Drug Likeness (ADMET) Predictions

Protox II webserver was used to predict nuclear receptor signaling pathways activation and other toxicity potentials of seven of the docked spirostans showing binding affinities comparable to that of exemestane, using the canonical SMILES of the molecules as input data. Ligand-based pharmacokinetics predictions were made for the aforementioned seven

spirostans and exemestane precisely by using the SwissADME webserver to predict their lipophilicity, water solubility, drug-likeness and bioavailability scores. Lipophilicity was measured as the consensus of iLOGP, XLOGP, MLOGP and Silicos-IT log P models of log P, the logarithm of partition coefficient of n-octanol/water partitioning system. Using the Silicos-IT model, water solubility was measured as the logarithm of molar concentration in water (Log S_w). Drug-likeness was predicted using Lipinsky rules of five (RO5), Verber's rules and bioavailability scores (Veber *et al*. 2002; Martin 2005; Pollastri 2010).

Aromatase-Ligand Complexes Simulations and Visualisations

Aromatase in complex with each of exemestane and the aforementioned seven spirostans was simulated and visualised using BIOVIA Discovery Studio Visualiser 2021 and UCSF Chimera 1.14 for respective 2D and 3D representations of interactions at the active site.

Molecular Dynamics Simulation

Molecular dynamics (MD) simulation of aromatase complex with digitogenin, the SS with the highest docking score, was performed with the aid of the Webgro macromolecular simulations webserver (https://simlab.uams.edu/) using 20 ns simulation time. Root mean square deviation (RMSD), root mean square fluctuation (RMSF) and radius of gyration (RG) of the trajectory were analysed to assess the stability of the complex.

RESULTS

QSAR

QSAR revealed high anti-proliferative tendencies for the 15 SS screened, showing probability ranges of 0.42–0.90 and 0.34–0.90 apoptosis agonism and anti-proliferative disease, respectively. Similarly, the predicted possible anti-neoplastic and specific anti-prostate cancer tendencies were very high, specific anti-BPH activity was modest while aromatase inhibitory activity probabilities were particularly low. The details of the QSAR predictions are presented in Table 1.

Aromatase Binding Affinities Predictions

With respect to the most stable binding pose of each compound, the co-crystallised ligand, exemestane, demonstrated a binding energy of -9.5 kcal/mol while the 46 SS (Table 2) demonstrated binding energies ranging from -9.9 kcal/mol to -5.3 kcal/mol. Seven of them, namely digitogenin (S/N 30, C1), manogenin (S/N 34, C2), ketotigogenin (S/N 4, C3), brisbagenin (S/N 20, C4), hecogenin (S/N 6, C5), spirost-1-en-3-one (S/N 24, C6) and yuccagenone (S/N 12, C7) with binding energies ranging from -9.9 kcal/mol to -9.0 kcal/mol were adjudged comparable to exemestane (S/N 1, C8) in binding affinity and thus considered for further in silico absorption, distribution, metabolism, excretion, toxicity (ADMET) and drug-likeness evaluations. Table 3 shows exemestane and the seven sapogenins with their respective number of PyRx search algorithm-generated poses and the binding energy of each compound's most stable pose.

Table 2: Pubchem identification numbers (PID) and names of aromatase (PDB ID 3s7s) co-crystalised inhibitor (S/N 1) and 46 spirostan sapogenins (S/N 2-47) randomly retrieved from the Pubchem chemical database (https://pubchem.ncbi.nlm.nih.gov/).

S/N	PID	Name	S/N	PID	Name
1	60198	Exemestane	25	255997	Soladulcidine
2	31342	Solancarpidine	26	330750	Epihippuristanol
3	65576	Tomatidine	27	330752	20-epihippurin
4	73682	Ketotigogenin	28	441880	Convallagenin
5	91439	Smilagenin	29	441881	Convallamarogenin
6	91453	Hecogenin	30	441886	Digitogenin
7	92095	Sarsasapogenin	31	441887	Gitogenin
8	99471	Solasodine diacetate	32	441893	Ruscogenin
9	99474	Diosgenin	33	441900	Yamogenin
10	99512	Epismailagenin	34	10253011	Manogenin
11	99516	Tigogenin	35	10529169	Tupichigenin
12	101692	Yuccagenone	36	10552033	Tupichigenin A
13	101906	Hecogenin acetate	37	10575379	Mexogenin
14	129125	Barbourgenin	38	10672322	Tupichigenin B
15	135760	6-methylspirost-5-en-3-ol	39	10717615	Ruizgenin
16	155860	Solagenin	40	10741302	Schidigeragenin
17	156656	Neosolaspigenin	41	10950372	Tupichigenin E
18	160498	Smilagenone	42	10973623	Tupichigenin Acetate
19	167555	Rockogenin	43	11518301	Anzurogenin A
20	167596	Brisbagenin	44	12303876	Convallagenin B
21	176535	Australigenin	45	16203751	Reineckiagenin A
22	177404	Spirostan-2,3,6-triol	46	21626039	Epiruscogenin
23	182281	Cannigenin	47	44559462	Ranmogenin A
24	191323	Spirost-1-en-3-one			

Table 3: Aromatase-binding energies of the best poses of exemestane (C8) and seven spirostan sapogenins (digitogenin, C1; manogenin, C2; ketotigogenin, C3; brisbagenin, C4; hecogenin, C5; spirost-1-en-3-one, C6 and yuccagenone, C7) of comparable aromatase binding energies to exemestane's.

Compound	Number of poses	Best pose binding energy (kcal/mol)
C8	9	−9.5
C1	2	−9.9
C2	2	−9.7
C3	2	−9.6
C4	3	−9.5
C5	2	−9.5
C6	4	−9.4
C7	4	−9.0

ERα-Binding Affinities

Re-docking estradiol to ERαLBD gave a very low binding energy (or high binding affinity), –10.7 kcal/mol. Exemestane, an established AI also showed a comparably high binding affinity (–8.2 kcal/mol). In contrast, all the seven spirostans showed relatively low binding affinities (–1.7 kcal/mol to –4.2 kcal/mol) to ERαLBD. These observations are summarised in Table 4.

Table 4: ERα-binding energies of the best poses of an ERα natural agonist, estradiol (C9); a typical aromatase inhibitor drug exemestane (C8) and seven spirostan sapogenins (digitogenin, C1; manogenin, C2; ketotigogenin, C3; brisbagenin, C4; hecogenin, C5; spirost-1-en-3-one, C6 and yuccagenone, C7) of comparable aromatase-binding energies to exemestane's.

Compound	Best pose binding energy (kcal/mol)
C9	–10.6
C8	–8.7
C1	–2.6
C2	–4.1
C3	–4.2
C4	–1.7
C5	–3.9
C6	–4.2
C7	–4.0

Nuclear Receptor-Associated and Other Toxicity Predictions

Evaluation of nuclear receptor signaling pathway interaction potentials of the compounds revealed that unlike exemestane, the seven SS were not active at any of the five implicated pathways, including the ERα (Table 5). Organ/end point and other toxicity predictions (Table 6) indicated that the seven SS did not show organ/end point toxicities with the exception of immunotoxicity, demonstrated also by exemestane.

ADME and Drug-Likeness Predictions

Drug-likeness predictive parameters—consensus log P, silicos-IT log S_w, Lipinsky violations, Verber violations and bioavailability scores—for exemestane and the seven spirostan sapogenins showing aromatase binding affinities comparable to exemestane's are as shown in Table 7. The Pharmacokinetic implications of these parameters on membrane permeation of these compounds are also summarised in Table 6, showing skin (log K_b), gastrointestinal (GI), blood brain barrier (BBB) permeations of the compounds in addition to their susceptibilities to cytochrome P450 (CYP) metabolising isozymes and P-glycoprotein efflux transporters.

Table 5: Predicted nuclear receptor signaling potentials of exemestane (C8) and seven spirostan sapogenins (digitogenin, C1; manogenin, C2; ketotigogenin, C3; brisbagenin, C4; hecogenin, C5; spirost-1-en-3-one, C6 and yuccagenone, C7) of comparable aromatase binding energies to exemestane's.

Compound	Nuclear receptor signaling pathways						
	AhR[a]	AR[b]	AR-LBD[c]	Arom[d]	ERα[e]	ER-LBD[f]	PPARγ[g]
C8	-	active	active	active	active	-	-
C1	-	-	-	-	-	-	-
C2	-	-	-	-	-	-	-
C3	-	-	-	-	-	-	-
C4	-	-	-	-	-	-	-
C5	-	-	-	-	-	-	-
C6	-	-	-	-	-	-	-
C7	-	-	-	-	-	-	-

Notes: [a]aryl hydrocarbon receptor; [b]androgen receptor; [c]androgen receptor ligand binding domain; [d]aromatase; [e]oestrogen receptor alpha; [f]oestrogen receptor ligand binding domain; [g]peroxisome proliferator activated receptor gamma.

Table 6: Predicted organ/end point toxicities of exemestane (C8) and seven spirostan sapogenins (digitogenin, C1; manogenin, C2; ketotigogenin, C3; brisbagenin, C4; hecogenin, C5; spirost-1-en-3-one, C6 and yuccagenone, C7) of comparable aromatase binding energies to exemestane's.

Compound	Organ/end point toxicities				
	Hepato toxicity	Carcinogenicity	Cytotoxicity	Immuno -toxicity	Mutagenicity
C8	-	-	-	Active	-
C1	-	-	-	Active	-
C2	-	-	-	Active	-
C3	-	-	-	Active	-
C4	-	-	-	Active	-
C5	-	-	-	Active	-
C6	-	-	-	Active	-
C7	-	-	-	Active	-

Table 7: Predicted drug likeness parameters: lipophilicity (log P), water solubility (Silicos-IT log Sw), Lipinsky and Verber violations, bioavailability scores of exemestane and seven spirostan sapogenins (digitogenin, C1; manogenin, C2; ketotigogenin, C3; brisbagenin, C4; hecogenin, C5; spirost-1-en-3-one, C6 and yuccagenone, C7) of comparable aromatase binding energies to exemestane's.

Molecule	Molecular weight	Consensus log P	Silicos-IT log S_w	Solubility class	Lipinsky #violations	Verber #violations	Bioavailability score
C8	296.4	3.51	−4.09	Moderately soluble	0	0	0.55
C1	448.64	3.27	−3.46	Soluble	0	0	0.55
C2	446.62	3.54	−3.56	Soluble	0	0	0.55
C3	430.62	4.39	−4.38	Moderately soluble	0	0	0.55
C4	432.64	4.40	−3.69	Soluble	1	0	0.55
C5	430.62	4.39	−4.38	Moderately soluble	0	0	0.55
C6	412.6	5.12	−4.74	Moderately soluble	1	0	0.55
C7	414.62	5.23	−5.2	Moderately soluble	1	0	0.55

2D Simulations of Aromatase-Ligand Interactions

There are observed variations in the type and number of amino acid residues the compounds interacted with at the enzyme's active site. Interaction types were however not as diverse, largely limited to hydrogen bonding, van der waals interactions and additional alkyl-alkyl and pi-alkyl interactions for the spirostans. Figures 4 and 5 depict the 2D simulations of active site interactions of C8, C1-C3 and C4-C7, respectively.

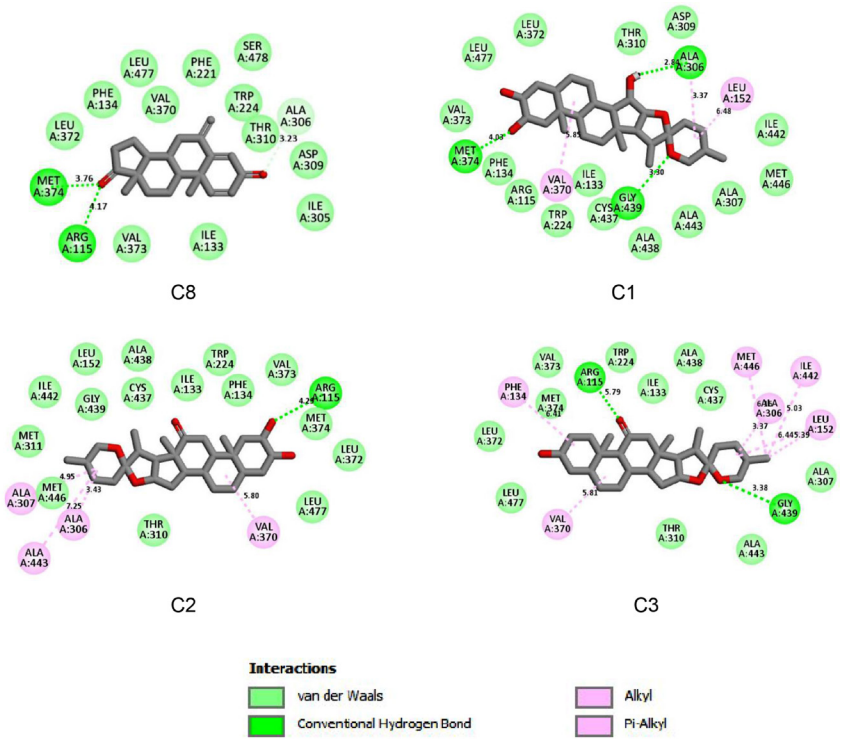

Figure 4: 2D simulations of intermolecular interactions of the most stable poses of C8 (exemestane), C1 (digitogenin), C2 (manogenin) and C3 (ketotigogenin) with aromatase active site amino acid residues.

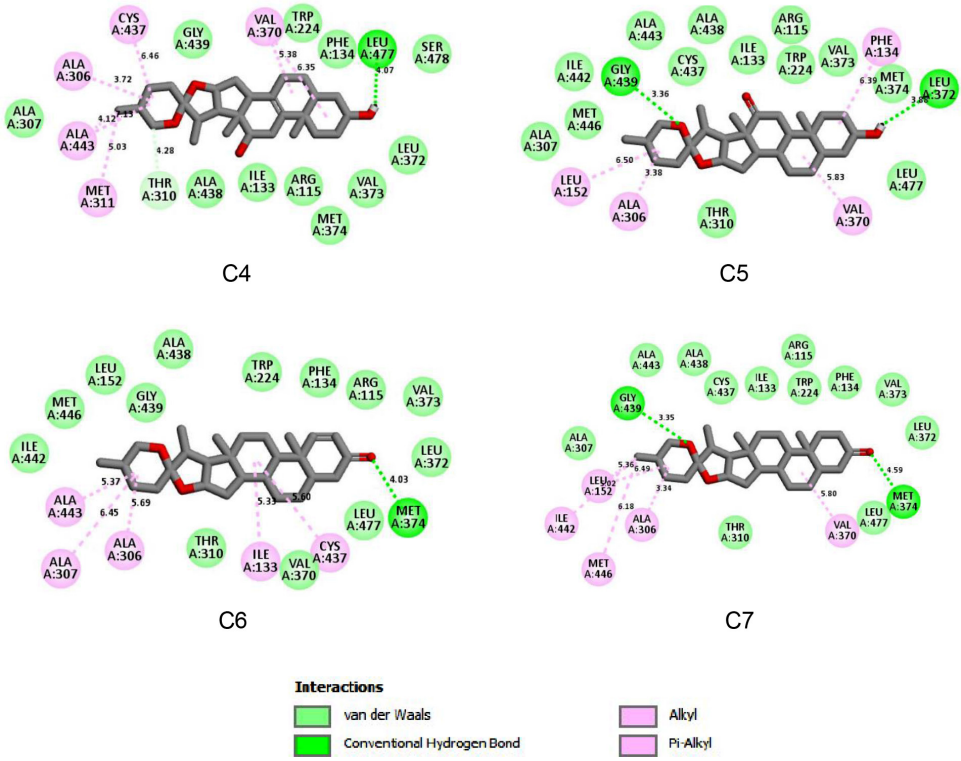

Figure 5: 2D simulations of intermolecula interactions of the most stable poses of C4 (brisbagenin), C5 (hecogenin), C6 (spirost-1en-3-one) and C7 (yuccagenone) with aromatase active site amino residues.

3D Simulations of Aromatase-Ligand Interactions

Marked variations were observed in the number of 3D poses generated by the PyRx conformational search algorithm: While nine poses were generated for exemestane (C8), four were generated for each of spirost-1-en-3-one (C6) and yuccagenone (C7), three for brisbagenin (C4) and two each for digitogenin (C1), manogenin (C2), ketotigogenin (C3) and hecogenin (C5). Figures 6, 7, 8 and 9, respectively, show the stick models of the PyRx conformational search algorithm-generated 3D poses of exemestane; spirost-1-en-3-one (C6) and yuccagenone (C7); brisbagenin (C4) and digitogenin (C1); manogenin (C2), ketotigogenin (C3) and hecogenin (C5) combinations, each showing the pose models (Ms) in decreasing order of docking scores or binding affinities to aromatase.

3D simulations of aromatase in complex with the best pose of each of the seven spirostans and exemestane showed the spirostans binding at the same location at the active site but with diverse conformations, explaining the differences noted in amino acid residues each compound interacted with. Figures 10, 11, 12 and 13, respectively, depict the 3D orientations of the best poses of exemestane and digitogeinin; manogenin and ketotigogenin; brisbagenin and hecogenin; spirost-1-en-3-one and yuccagenone at the aromatase active site binding pocket shown in both solid and transparent surface modes.

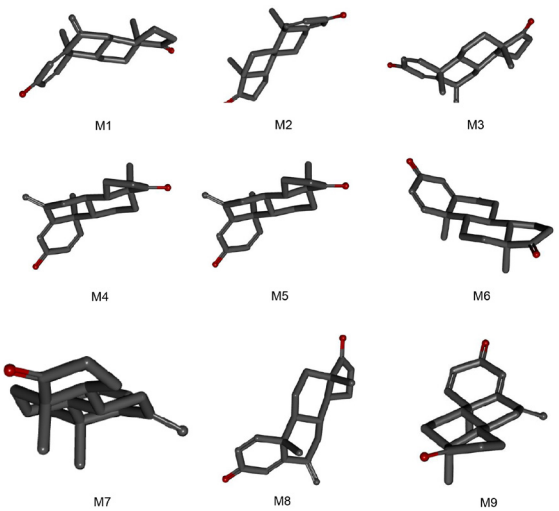

Figure 6: 3D stick models of PyRx-generated C8 (exemestane) poses (M1–M9) in decreasing order of binding affinity to aromatase.

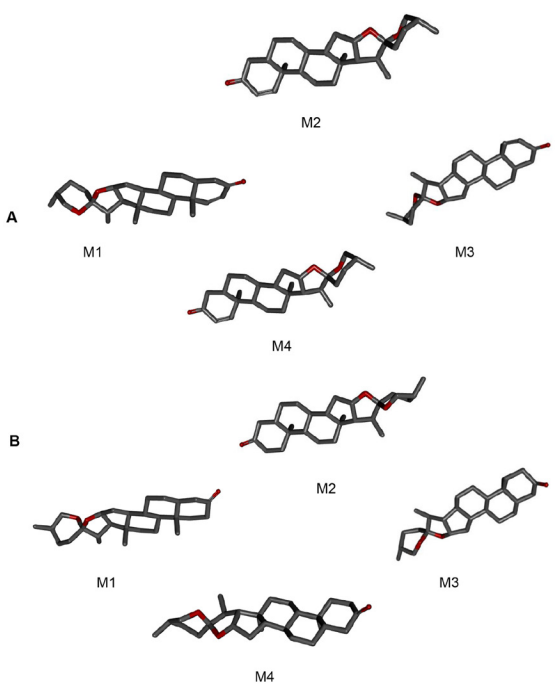

Figure 7: 3D stick models of PyRx-generated poses of A: spirost-1-en-3-one (C6) poses (M1–M4) and B: yuccagenone (C7) poses (M1–M4), both in decreasing order of binding affinity to aromatase.

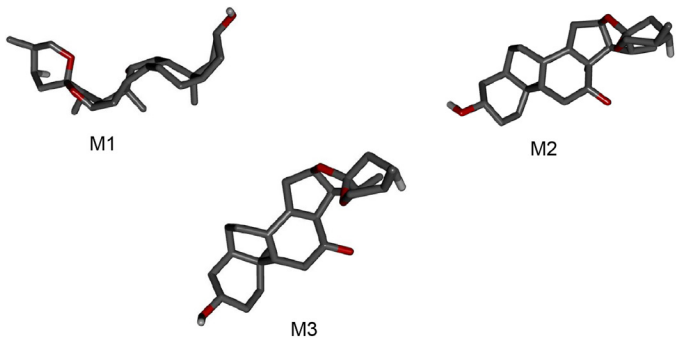

Figure 8: 3D stick models of PyRx-generated brisbagenin (C4) poses (M1–M3) in decreasing order of binding affinity to aromatase.

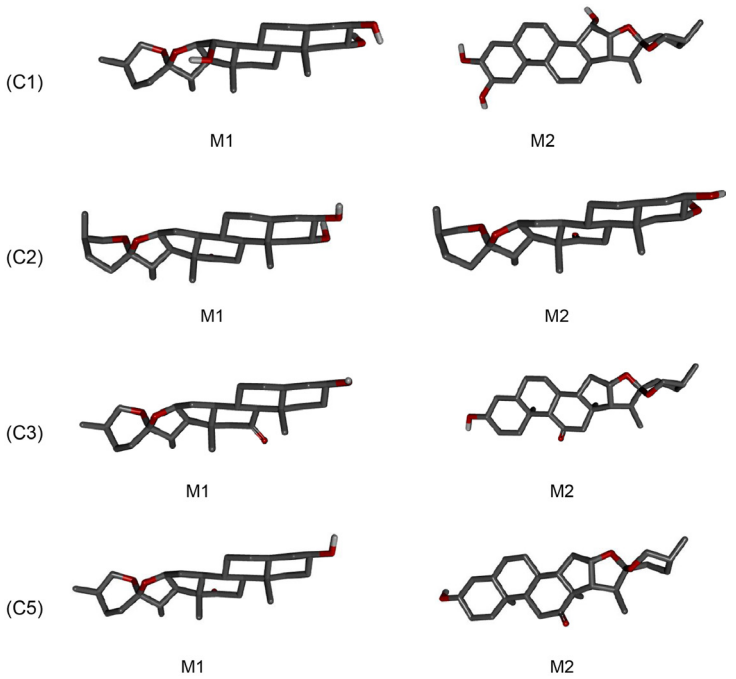

Figure 9: Three dimensional stick models of PyRx-generated poses of: digitogenin (C1) (M1–M2); manogenin (C2) (M1–M2); ketotigogenin (C3) (M1–M2) and hecogenin (C5) (M1–M2), all in decreasing order of binding affinity to aromatase.

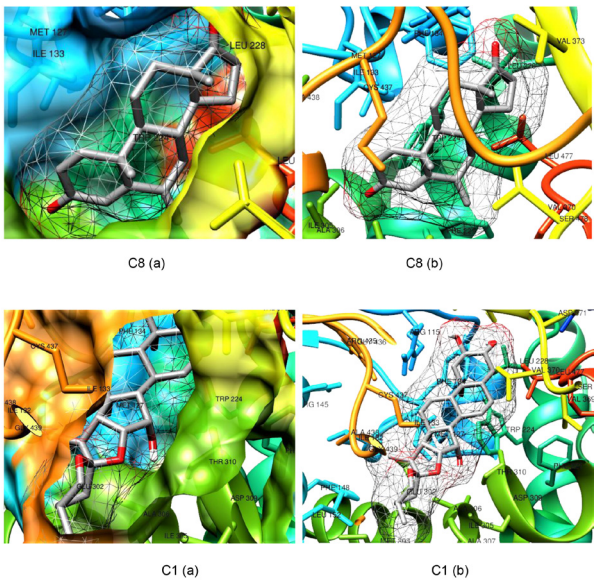

Figure 10: 3D simulation of the most stable poses of exemestane (C8) and digitogenin (C1) in the aromatase active site binding pocket shown in the surface (a) and transparent (b) modes.

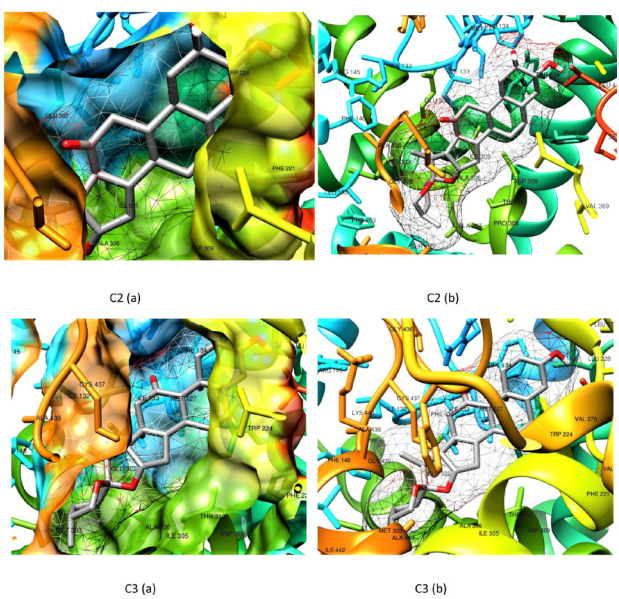

Figure 11: 3D simulations of the most stable poses of manogenin (C2) and ketotigogenin (C3) in the aromatase active site binding pocket shown as solid (a) and transparent (b) surfaces.

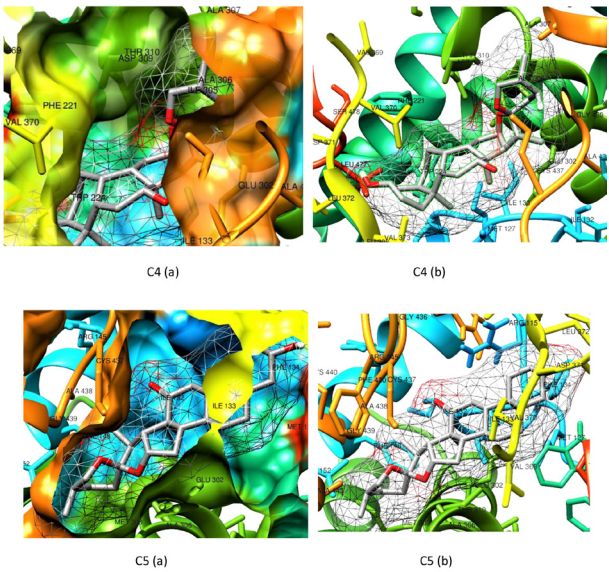

Figure 12: 3D simulations of the most stable poses of brisbagunin (C4) and hecogenin (C5) in the aromatase active site binding pocket shown as solid (a) and transparent (b) surfaces.

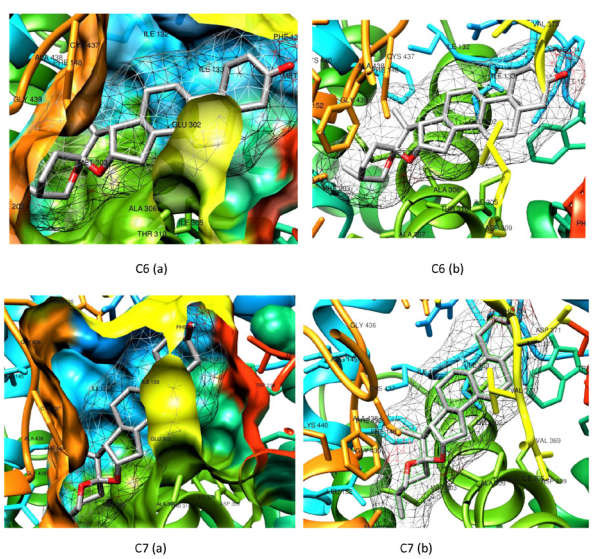

Figure 13: 3D simulations of the most stable poses of spirost-1-en-3-one (C6) and yuccagenone (C7) in the aromatase active site binding pocket shown as solid (a) and transparent (b) surfaces.

Molecular Dynamics (MD) Simulation Results

The RMSD, RMSF and RG trajectory analyses results of the simulation are as shown in Figure 14.

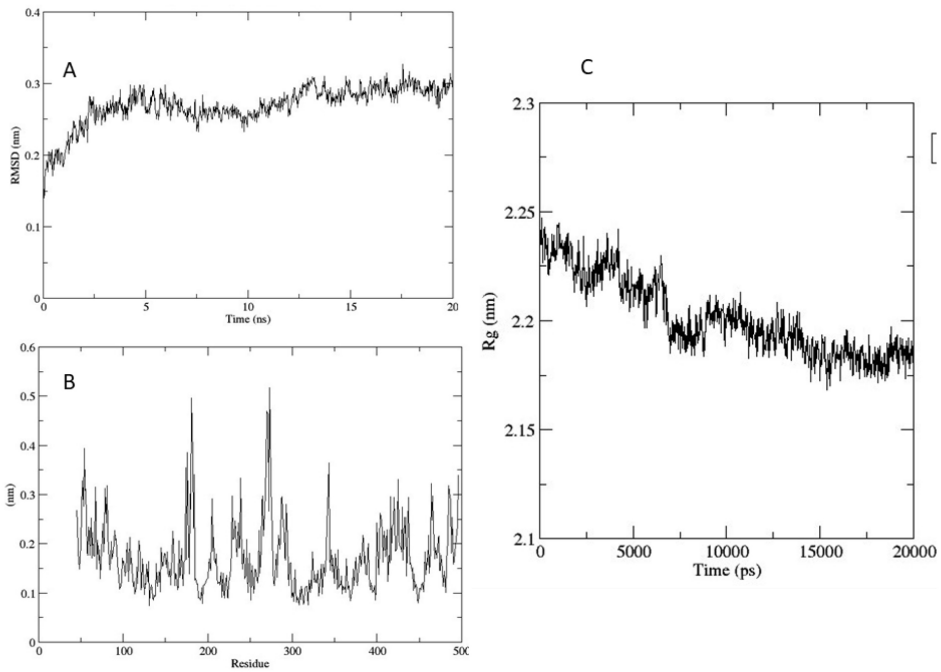

Figure 14: RMSD (A); RMSF (B) and radius of gyration (C) analyses of aromatase-digitogenin complex dynamics trajectory run over 20 ns simulation time.

DISCUSSION

QSAR Predictions

Table 1 reveals high probability ranges for the anti-proliferative disease (0.34–0.90) and apoptosis agonism (0.42–0.90) activities, implying high anti-proliferative tendencies supportive of the anti-BPH conjecture. The modest probability ranges observed for specific anti-BPH (0.26–0.41) and other anti-prostate disorders (0.31–0.41) tendencies were equally supportive of the anti-BPH conjecture. And though, the rather low probability range (0.05–0.20) for the aromatase inhibitory activity was, on the face value, not supportive of the proposed aromatase inhibitory anti-BPH mechanism, it was interpreted with caution to mean neither low activity nor inactivity. This is because ligand-based webserver QSAR algorithms are expected to be weak in action mechanism predictions, as they make use of 1D (canonical SMILES) and/or 2D models of compounds, ignoring the crucial roles that 3D

configuration and conformations play in their biological activities (Banegas-Luna, Cerón-Carrasco and Pérez-Sánchez 2018). In other words, a low-value action mechanism QSAR prediction may result from inaccessibility of webserver's algorithm to ligand's bioactive structural conformation. A combination of low AI and high anti-proliferative potentials was, therefore, considered enough impetus for the structure-based *in silico* aromatase inhibitory anti-BPH screening, which, in any case, would be more reliable, as it is not only based on ligands' 3D structures, but also on their bioactive conformations (Wang *et al*. 2018).

Selective Aromatase Inhibition by Spirostans

The conjecture that spirostans would have high tendencies of aromatase binding on the basis of their steroidal structure mimicry of the enzyme's natural substrates is proven by their display of relatively high docking scores (corresponding to high negative binding energies), with some as high as that of the co-crystalised ligand and some, even higher (Table 3). The relative high-affinity binding of seven of the docked spirostans, with binding energies (ranging from –9.9 kcal/mol to –9.0 kcal/mol) comparable to –9.5 kcal/mol binding energy for the co-crystalised inhibitor, exemestane, is presumable as competitively inhibitory, though non-competitive inhibition could not be ruled out (Blat 2010). However, the outstanding feature of the aromatase-spirostan interaction garnered from this investigation is not merely that of inhibition but rather more of an associated selectivity decipherable from the results of the ligand-based ADMET evaluations depicted in Tables 4–8. Expectedly, exemestane activated all the nuclear signaling pathways, including ERα and aromatase itself, indiscriminately. On the contrary, none of the seven aforementioned spirostans showed activation of any of the nuclear receptor signaling pathways. The relative low affinities of these seven spirostans (–1.7 kcal/mol to –4.2 kcal/mol) compared to those of estradiol (–10.7 kcal/mol) and exemestane (–8.7 kcal/mol) in the ERαLBD docking experiment corroborated this observed nuclear receptor-sparing selectivity (Tables 4 and 5). Though the unique electronic and stereochemical features of the spirostans could contribute significantly to this observed selectivity, steric encumbrance contributions of their relative huge structures and molecular weights (Figure 2 and Table 7) appear more vivid and plausible, predicating on spirostans' hindered access/degree of freedom at the macromolecular active site and/or interference of their non-pharmacophoric structural features with important receptor interactions (Patrick 2013).

Potential Organ/End Point Toxicity of Spirostan Sapogenins

Organ/end point toxicity predictions showed the seven sapogenins to demonstrate potential immunotoxicity (Table 6). However, the fact that this was also demonstrated by exemestane, an aromatase inhibitor already in clinical use, suggests this potential toxicity to be either inconsequential or tolerable. In any case, immunotoxicity should be noted as a potential end point toxicity for spirostans and subjected to mitigation by molecular modification protocols, if needs be.

Drug-likeness and ADME—log P and log S_w, Bioavailability Scores

Drug likeness is a qualitative/semi-quantitative assessment of the possibility of oral activity of a drug based on bioavailability (Daina, Michielin and Zoete 2017). Indeed, a hydrophilicity/lipophilicity balance is required for optimum ADME profiles required for oral bioavailability. Drug likeness is therefore assessed based on an integrated interpretation of lipophilicity/

hydrophilicity parameters like log P and water solubility (log S) alongside data from some rule-based filter models, notable amongst which are Lipinski and Verber rules (Veber *et al*. 2002; Pollastri 2010).

SwissADME predicts log P using five predictor models (iLOGP, XLOGP, WLOGP, MLOGP, Silicos-IT log P) and their consensus. Likewise, it uses three solubility predictors (ESOL, Ali and Silicos-IT) to predict water solubility (Daina, Michielin and Zoete 2017). The consensus (or average) of the five log P models and Silicos-IT log S_w are shown in Table 6. A careful analysis of the consensus log P values shows that both the seven sapogenins and exemestane could be adjudged optimally lipophilic as none of them gave a consensus log P value of up to 5.5, the threshold value above which compounds are generally adjudged too lipophilic for oral activity and, as such, too water insoluble to be available for absorption or distribution (Silverman 2012). It is however worthy of note that digitogenin (C1) and manogenin (C2) gave low consensus log P values (3.27 and 3.54, respectively) comparable to that of exemestane (3.51), despite significant additional hydrocarbon residues. The Silicos-IT water solubility predictor showed each of the seven spirostans under consideration and exemestane as either soluble or moderately soluble in water, indicating a modest hydrophilicity in tandem with what is indirectly predictable from its lipophilicity (log P).

The Lipinski rules of five states that an orally bioavailable drug must neither possess more than five hydrogen bond donors nor more than 10 hydrogen bond acceptors; its molecular weight must not be greater than 500 g/mol and its log P value not greater than 5. The Lipinski filter requires that an orally bioavailable drug must not violate more than one of these four postulates (Pollastri 2010). On another hand, the Verber filter requires that an orally bioavailable agent must neither have more than 10 rotatable bonds nor possess a polar surface area greater than 140 $Å^2$ (Veber *et al*. 2002). A careful analysis of the outcome of subjecting the compounds (C1–C8) to these filters shows that both the spirostans of interest and exemestane are drug-like agents as none violated more than one Lipinski rule or any of the Verber rules. In addition, they all also had their drug likeness parameters ultimately agreeing with their SwissADME-assigned bioavailability scores (Table 6). Bioavailability score is assigned as the probability of 10% oral bioavailability in rat or human colon carcinoma (Caco) cells. The bioavailability scores for each of the seven sapogenins and exemestane was 0.55, indicating that each of them has at least 55% probability of having 10% oral bioavailability in rat or Caco-2 cells, which is good for moderate oral bioavailability (Martin 2005).

Pharmacokinetic Behaviours—Membrane Permeation, Metabolising Enzymes and Transport Protein Susceptibilities

Polar/hydrophilic xenobiotics are screened off biological systems by lipophilic biological membranes, substrates of influx proteins being exceptions (Yang and Hinner 2015). In like manner, the human body has evolved metabolising enzymes and efflux membrane transporters to rid itself of non-polar/moderately polar substances to which the lipid membranes are pervious. Unfortunately, drugs, being extraneous, are subjected to the same evolutionary alliance of metabolic and efflux transporter clearance aimed at ridding the body of extraneous substances (Chan, Lowes and Hirst 2004; Murakami and Takano 2008). Membrane permeation, metabolising enzymes as well as efflux transporter proteins susceptibilities are therefore critical to internal xenobiotic concentration the body is exposed to and, hence, are of special consideration in the early stages of drug development to reduce pharmacokinetic-related failure rate in drug development. In addition, xenobiotic metabolism and efflux transport is implicated in drug-drug and drug-food interactions as the

proteins involved can either be induced or inhibited (Pal and Mitra 2006). Table 8 shows all the compounds, including exemestane, to be lipophilic enough to demonstrate high gastrointestinal (GI) absorption. Likewise, all, with the exception of spirost-1-en-3-one (C6), permeated the blood brain barrier (BBB), indicating possibility of central toxicity and, hence, caution with their clinical use if unmodified. All of them also demonstrated negative log Kp portending their ready skin permeation and, hence, potentials for percutaneous route of administration (Potts and Guy 1992).

CYP is the most important superfamily of phase 1 metabolising enzymes for drugs and xenobiotics (Anzenbacher and Anzenbacherova 2001). At least 57 isoforms of CYP have been characterised but only the most important five (CYP1A2, CYP2C19, CYP2C9, CYP2D6, CYP3A4) of the few linked with drug metabolism (Anzenbacher and Anzenbacherova 2001; Olsen, Oostenbrink and Jørgensen 2015) are considered in SwissADME. Table 8 shows that while exemestane is a substrate of CYP2C19 and CYP2C9 isoforms, none of the seven sapogenins is a substrate of any of these five important isoforms of CYP, ruling out drug-drug interaction that could result from induction or inhibition of their metabolisms (Bohnert *et al.* 2016). Cautions should however be exercised to avoid over-interpreting this as meaning that these spirostans are free from drug interactions as the results do not show that the spirostans themselves could not induce or inhibit metabolism of other xenobiotics. Additional in silico models would be required to make such predictions in the affirmative.

P-glycoprotein (Pgp) is a membrane efflux transporter belonging to the ATP-binding cassette (ABC) protein superfamily. It first became popular when its overexpression in cancer cells was discovered to be responsible for the multidrug resistance phenomenon in cancer chemotherapy (Gottesman, Pastan and Ambudkar 1996). Its expression in normal tissues like the small intestine, liver, BBB and kidneys which, in some ways, are connected with absorption, distribution and elimination of xenobiotics, has nevertheless underscored their importance in pharmacokinetics, drug-drug, drug-food and drug-herb interactions (Lin and Yamazaki 2003). P-gp effluxes chemical substances of diverse molecular structures out of cells into lumens or extracellular spaces. Its activities invariably leads to impaired GI absorption, reduced concentration of xenobiotics in the central nervous system (CNS) and increased biliary and renal elimination of same, all amounting to poor bioavailability of Pgp substrates. Table 8 shows that exemestane is not a Pgp substrate. Its bioavailability would therefore be both uncompromisable by Pgp and unresponsive to Pgp inducers or inhibitors. On the other hand, five of the spirostans, digitogenin, manogenin, ketotigogenin, brisbagenin and hecogenin (C1–C5), are Pgp substrates while two, spirost-1-en-3-one and yuccagenone (C6 and C7), are not, indicating that compounds C1–C5 would most likely be objects of drug-drug or drug-herb interactions.

Aromatase-Ligand Interactions Simulation

There is at least one hydrogen bonding interaction demonstrated by each of the compounds but not to one particular amino acid residue (Figures 4 and 5). And though the additional alkyl-alkyl and pi-alkyl interactions seen only with the spirostans did not amount to increased binding affinity, they might, nevertheless, be contributory to the observed spirostan selectivity as they could have significant effects on overall aromatase-ligand complex conformation. The final aromatase-ligand complex conformation would certainly determine the number and topography of allosteric sites, the secondary binding to which might have modulatory effects on the enzyme's inhibition consequences (Skjærven, Reuter and Martinez 2011). Moreover, the observed variation in type and number of amino acid residues to which the compounds showed interactions at the enzyme's active site is an indication of the

latter's large volume (Ghosh *et al*. 2009; 2010) and differences in the 3D orientations of the compounds as illustrated with the variations in the 3D orientations of their most stable conformations in Figures 10, 11, 12 and 13.

Table 8: Pharmacokinetic behaviours/outcomes – Membrane permeations, CYP metabolism and Pgp efflux transport susceptibilities of exemestane (C8) and seven spirostan sapogenins (digitogenin, C1; manogenin, C2; ketotigogenin, C3; brisbagenin, C4; hecogenin, C5; spirost-1-en-3-one, C6 and yuccagenone, C7) of comparable aromatase binding energies to exemestane's.

Molecule	GI absorption	BBB permeant	log Kp (cm/s)	CYP 1A2	CYP 2C19	CYP 2C9	CYP 2D6	CYP 3A4	Pgp substrate
C8	High	Yes	−5.93	No	Yes	Yes	No	No	No
C1	High	Yes	−6.71	No	No	No	No	No	Yes
C2	High	Yes	−6.29	No	No	No	No	No	Yes
C3	High	Yes	−5.47	No	No	No	No	No	Yes
C4	High	Yes	−5.02	No	No	No	No	No	Yes
C5	High	Yes	−5.5	No	No	No	No	No	Yes
C6	High	Yes	−4.37	No	No	No	No	No	No
C7	High	No	−4.52	No	No	No	No	No	No

Molecular Dynamics and Stability of Aromatase-Digitogenin Complex

RMSD analysis (Figure 14A) shows that the structure converged at around 2.5 ns and remained largely stable throughout the 20 ns simulation time, deviating from the initial structure within only 2 Å–3 Å. A general model fluctuation pattern by most residues is decipherable from the RMSF which, nevertheless, also revealed a couple of regions with highly flexible residues (Figure 14B), but largely maintaining the radius of gyration around 22 Å. These stability-implicative parameters (Kumar *et al*. 2019; Uddin *et al*. 2019) could be taken as representative of the SS chemical space, given their structural similarities (Figure 2).

CONCLUSION

Oestrogen ablation as a clinical application of the knowledge of oestrogen involvement in BPH establishment and progression is actually possible via AI provided selectivity is achieved by using agents that would inhibit aromatase without activating the signaling pathways of proteins in the nuclear receptor superfamily, especially the ERα. This investigation, via both structure-based and ligand-based *in silico* means, has uncovered seven spirostan sapogenins that could do just this. The seven spirostan sapogenins herein reported could therefore become candidates for further *in-vitro*, *in-vivo* and molecular modification investigations aimed at the discovery of clinically applicable anti-oestrogen anti-BPH agents.

ACKNOWLEDGEMENTS

The authors wish to acknowledge the management of the Faculty of Pharmacy, University of Lagos for providing an enabling research environment.

REFERENCES

ANDRIOLE, G., BRUCHOVSKY, N., CHUNG, L. W., MATSUMOTO, A. M., RITTMASTER, R., ROEHRBORN, C. & TINDALL, D. (2004) Dihydrotestosterone and the prostate: The scientific rationale for 5α-reductase inhibitors in the treatment of benign prostatic hyperplasia, *The Journal of Urology*, 172(4 Part 1): 1399–1403. https://doi.org/10.1097/01.ju.0000139539.94828.29

ANZENBACHER, P. & ANZENBACHEROVA, E. (2001) Cytochromes P450 and metabolism of xenobiotics, *Cellular and Molecular Life Sciences*, 58(5): 737–747. https://doi.org/10.1007/PL00000897

BARAKAT, R., OAKLEY, O., KIM, H., JIN, J. & KO, C. J. (2016) Extra-gonadal sites of estrogen biosynthesis and function, *BMB Reports*, 49(9): 488–496. https://doi.org/10.5483/BMBRep.2016.49.9.141

BANEGAS-LUNA, A. J., CERÓN-CARRASCO, J. P. & PÉREZ-SÁNCHEZ, H. (2018) A review of ligand-based virtual screening web tools and screening algorithms in large molecular databases in the age of big data, *Future Medicinal Chemistry*, 10(22): 2641–2658. https://doi.org/10.4155/fmc-2018-0076

BECHIS, S. K., OTSETOV, A. G., GE, R. & OLUMI, A. F. (2014) Personalized medicine for the management of benign prostatic hyperplasia, T*he Journal of Urology*, 192(1): 16–23. https://doi.org/10.1016/j.juro.2014.01.114

BHAT, S. V., NAGASAMPAGI, B. A. & SIVAKUMAR, M. (2005) Chemistry of natural products, pp. 108–110 (New York: Springer).

BOHNERT, T., PATEL, A., TEMPLETON, I., CHEN, Y., LU, C., LAI, G. et al. (2016) Evaluation of a new molecular entity as a victim of metabolic drug-drug interactions—an industry perspective, *Drug Metabolism and Disposition*, 44(8): 1399–1423. https://doi.org/10.1124/dmd.115.069096

BLAT, Y. (2010) Non-competitive inhibition by active site binders, *Chemical Biology & Drug Design*, 75(6), 535–540. https://doi.org/10.1111/j.1747-0285.2010.00972.x

CHAN, L. M., LOWES, S. & HIRST, B. H. (2004) The ABCs of drug transport in intestine and liver: Efflux proteins limiting drug absorption and bioavailability, *European Journal of Pharmaceutical Sciences*, 21(1): 25–51. https://doi.org/10.1016/j.ejps.2003.07.003

DAINA, A., MICHIELIN, O. & ZOETE, V. (2017) SwissADME: A free web tool to evaluate pharmacokinetics, drug-likeness and medicinal chemistry friendliness of small molecules, *Scientific Reports*, 7(1): 1–13. https://doi.org/10.1038/srep42717

DAVID, L., THAKKAR, A., MERCADO, R. & ENGKVIST, O. (2020) Molecular representations in AI-driven drug discovery: A review and practical guide, *Journal of Cheminformatics*, 12(1): 1–22. https://doi.org/10.1186/s13321-020-00460-5

ELKAHWAJI, J. E. (2013) The role of inflammatory mediators in the development of prostatic hyperplasia and prostate cancer, *Research and Reports in Urology*, 5: 1–10. https://doi.org/10.2147/RRU.S23386

ELLEM, S. J. & RISBRIDGER, G. P. (2009) The dual, opposing roles of estrogen in the prostate, *Annals of the New York Academy of Sciences*, 1155(1): 174–186. https://doi.org/10.1111/j.1749-6632.2009.04360.x

ETREBY, M. F. E., NISHINO, Y., HABENICHT, U. F. & HENDERSON, D. (1991) Atamestane, a new aromatase inhibitor for the management of benign prostatic hyperplasia, *Journal of Andrology*, 12(6): 403–414.

FLÅGENG, M. H., HAUGAN MOI, L. L., DIXON, J. M., GEISLER, J., LIEN, E. A., MILLER, W. R. et al. (2009) Nuclear receptor co-activators and HER-2/neu are upregulated in breast cancer patients during neo-adjuvant treatment with aromatase inhibitors, *British Journal of Cancer*, 101(8): 1253–1260. https://doi.org/10.1038/sj.bjc.6605324

FUJII, R., HANAMURA, T., SUZUKI, T., GOHNO, T., SHIBAHARA, Y., NIWA, T. et al. (2014) Increased androgen receptor activity and cell proliferation in aromatase inhibitor-resistant breast carcinoma, *The Journal of Steroid Biochemistry and Molecular Biology*, 144: 513–522. https://doi.org/10.1016/j.jsbmb.2014.08.019

GAILLARD, S. & STEARNS, V. (2011) Aromatase inhibitor-associated bone and musculoskeletal effects: New evidence defining etiology and strategies for management, *Breast Cancer Research*, 13(2): 1–11. https://doi.org/10.1186/bcr2818

GHOSH, D., GRISWOLD, J., ERMAN, M. & PANGBORN, W. (2009) Structural basis for androgen specificity and oestrogen synthesis in human aromatase, *Nature*, 457(7226): 219–223. https://doi.org/10.1038/nature07614

GHOSH, D., GRISWOLD, J., ERMAN, M. & PANGBORN, W. (2010) X-ray structure of human aromatase reveals an androgen-specific active site, *The Journal of Steroid Biochemistry and Molecular Biology*, 118(4–5): 197–202. https://doi.org/10.1016/j.jsbmb.2009.09.012

GOTTESMAN, M. M., PASTAN, I. & AMBUDKAR, S. V. (1996) P-glycoprotein and multidrug resistance, *Current Opinion in Genetics and Development*, 6(5): 610–617. https://doi.org/10.1016/s0959-437x(96)80091-8

HANAMURA, T. & HAYASHI S. (2018) Overcoming aromatase inhibitor resistance in breast cancer: Possible mechanisms and clinical applications, *Breast Cancer*, 25(4): 379–391. https://doi.org/10.1007/s12282-017-0772-1

HENDERSON, D., HABENICHT, U. F., NISHINO, Y. & EL ETREBY, M. F. (1987). Estrogens and benign prostatic hyperplasia: the basis for aromatase inhibitor therapy, *Steroids*, 50(1–3): 219–233. https://doi.org/10.1016/0039-128X(83)90073-9

HENDERSON, D. (1987) Aromatase inhibitors: Their biochemistry and clinical potential, *Journal of Steroid Biochemistry*, 27(4–6): 905–914. https://doi.org/10.1016/0022-4731(87)90167-1

HIRSHBURG, J. M., KELSEY, P. A., THERRIEN, C. A., GAVINO, A. C. & REICHENBERG, J. S. (2016) Adverse effects and safety of 5-alpha reductase inhibitors (finasteride, dutasteride): A systematic review, *The Journal of Clinical and Aesthetic Dermatology*, 9(7): 56–62.

HO, C. K. & HABIB, F. K. (2011) Estrogen and androgen signaling in the pathogenesis of BPH, *Nature Reviews Urology*, 8(1): 29–41. https://doi.org/10.1038/nrurol.2010.207

HOWELL, A. & CUZICK, J. (2005) Vascular effects of aromatase inhibitors: Data from clinical trials, *The Journal of Steroid Biochemistry and Molecular Biology*, 95(1–5): 143–149. https://doi.org/10.1016/j.jsbmb.2005.04.005

KAPLAN, S. A., O'NEILL, E., LOWE, R., HANSON, M. & MEEHAN, A. G. (2013) Prevalence of low testosterone in aging men with benign prostatic hyperplasia: Data from the Proscar Long-term Efficacy and Safety Study (PLESS), *The Aging Male*, 16(2): 48–51. https://doi.org/10.3109/13685538.2013.773421

KUMAR, N., SOOD, D., TOMAR, R. & CHANDRA, R. (2019) Antimicrobial peptide designing and optimization employing large scale flexibility analysis of protein-peptide fragments, *ACS Omega*, 4(25): 21370–21380. https://doi.org/10.1021/acsomega.9b03035

LA VIGNERA, S., CONDORELLI, R. A., RUSSO, G. I., MORGIA, G. & CALOGERO, A. E. (2016) Endocrine control of benign prostatic hyperplasia, *Andrology*, 4(3): 404–411. https://doi.org/10.1111/andr.12186

LOKESHWAR, S. D., HARPER, B. T., WEBB, E., JORDAN, A., DYKES, T. A., NEAL Jr, D. E. et al. (2019) Epidemiology and treatment modalities for the management of benign prostatic hyperplasia, *Translational Andrology and Urology*, 8(5): 529–539. https://doi.org/10.21037/tau.2019.10.01

LIN, J. H. & YAMAZAKI, M. (2003) Role of P-glycoprotein in pharmacokinetics: Clinical implications, *Clinical Pharmacokinetics*, 42(1): 59–98. https://doi.org/10.2165/00003088-200342010-00003

LUI, A., NEW, J., OGONY, J., THOMAS, S. & LEWIS-WAMBI, J. (2016) Everolimus downregulates estrogen receptor and induces autophagy in aromatase inhibitor-resistant breast cancer cells, *BMC Cancer*, 16(1): 1–15. https://doi.org/10.1186/s12885-016-2490-z

MARTIN, Y. C. (2005) A bioavailability score, *Journal of Medicinal Chemistry*, 48(9): 3164–3170. https://doi.org/10.1021/jm0492002

MITWALLY, M. F. & CASPER, R. F. (2006) Potential of aromatase inhibitors for ovulation and superovulation induction in infertile women, *Drugs*, 66(17): 2149–2160. https://doi.org/10.2165/00003495-200666170-00001

MONTIRONI, R., VALLI, M. & FABRIS, G. (1996) Treatment of benign prostatic hyperplasia with 5-alpha-reductase inhibitor: Morphological changes in patients who fail to respond, *Journal of Clinical Pathology*, 49(4): 324–328. https://doi.org/10.1136/jcp.49.4.324

MURAKAMI, T. & TAKANO, M. (2008) Intestinal efflux transporters and drug absorption, *Expert Opinion on Drug Metabolism and Toxicology*, 4(7): 923–939. https://doi.org/10.1517/17425255.4.7.923

OLSEN, L., OOSTENBRINK, C. & JØRGENSEN, F. S. (2015) Prediction of cytochrome P450 mediated metabolism, *Advanced Drug Delivery Reviews*, 86: 61–71. https://doi.org/10.1016/j.addr.2015.04.020

PAL, D. & MITRA, A. K. (2006) MDR-and CYP3A4-mediated drug–drug interactions, *Journal of Neuroimmune Pharmacology*, 1(3): 323–339. https://doi.org/10.1007/s11481-006-9034-2

PATRICK G. L. (2013) An introduction to medicinal chemistry, 5th edition, pp. 236–238 (Oxford: Oxford University Press).

PAVONE, M. E. & BULUN, S. E. (2012) Aromatase inhibitors for the treatment of endometriosis, *Fertility and Sterility*, 98(6):1370–1379. https://doi.org/10.1016/j.fertnstert.2012.08.053

POLLASTRI, M. P. (2010) Overview on the Rule of Five, *Current Protocols in Pharmacology*, 49(1): 9–12. https://doi.org/10.1002/0471141755.ph0912s49

POTTS, R. O. & GUY, R. H. (1992) Predicting skin permeability, *Pharmaceutical Research*, 9(5): 663–669. https://doi.org/10.1023/A:1015810312465

RASTRELLI, G., VIGNOZZI, L., CORONA, G. & MAGGI, M. (2019) Testosterone and benign prostatic hyperplasia, *Sexual Medicine Reviews*, 7(2): 259–271. https://doi.org/10.1016/j.sxmr.2018.10.006

SABALE, P. M., SABALE, V. P. & POTEY, L. C. (2018) Aromatase and aromatase inhibitors in breast cancer treatment, *Journal of Current Pharma Research*, 9(1): 2636–2655. https://doi.org/10.33786/JCPR.2018.v09i01.008

SAENGMEARNUPARP, T., LOJANAPIWAT, B., CHATTIPAKORN, N. & CHATTIPAKORN, S. (2021) The connection of 5-alpha reductase inhibitors to the development of depression, *Biomedicine and Pharmacotherapy*, 143: 112100. https://doi.org/10.1016/j.biopha.2021.112100

SCIARRA, A., MARIOTTI, G., SALCICCIA, S., GOMEZ, A. A., MONTI, S., TOSCANO, V. et al. (2008) Prostate growth and inflammation, *The Journal of Steroid Biochemistry and Molecular Biology*, 108(3–5): 254–260. https://doi.org/10.1016/j.jsbmb.2007.09.013

SÉRALINI, G. E. & MOSLEMI, S. (2001) Aromatase inhibitors: Past, present and future, *Molecular and Cellular Endocrinology*, 178(1–2): 117–131. https://doi.org/10.1016/S0303-7207(01)00433-6

SILVERMAN, R. B. (2012) The organic chemistry of drug design and drug action, 2nd edition, pp. 51–63 (Toronto: Elsevier).

SKJÆRVEN, L., REUTER, N. & MARTINEZ, A. (2011) Dynamics, flexibility and ligand-induced conformational changes in biological macromolecules: A computational approach, *Future Medicinal Chemistry*, 3(16): 2079–2100. https://doi.org/10.4155/fmc.11.159

TROST, L., SAITZ, T. R. & HELLSTROM, W. J. (2013) Side effects of 5-alpha reductase inhibitors: A comprehensive review, *Sexual Medicine Reviews*, 1(1): 24–41. https://doi.org/10.1002/smrj.3

UDDIN, M. Z., LI, X., JOO, H., TSAI, J., WRISCHNIK, L. & JASTI, B. (2019) Rational design of peptide ligands based on knob-socket protein packing model using CD13 as a prototype receptor, *ACS Omega*, 4(3): 5126–5136. https://doi.org/10.1021/acsomega.8b03421

VEBER, D. F., JOHNSON, S. R., CHENG, H. Y., SMITH, B. R., WARD, K. W. & KOPPLE, K. D. (2002) Molecular properties that influence the oral bioavailability of drug candidates, *Journal of Medicinal Chemistry*, 45(12): 2615–2623. https://doi.org/10.1021/jm020017n

WANG, X., SONG, K., LI, L. & CHEN, L. (2018) Structure-based drug design strategies and challenges, *Current Topics in Medicinal Chemistry*, 18(12): 998–1006. https://doi.org/10.2174/1568026618666180813152921

YANG, N. J. & HINNER, M. J. (2015) Getting across the cell membrane: An overview for small molecules, peptides, and proteins, *Methods in Molecular Biology (Clifton, N.J.)*, 1266: 29–53. https://doi.org/10.1007/978-1-4939-2272-7_3